Thermal conductivity of a single Bi$_{0.5}$Sb$_{1.5}$Te$_3$ single-crystalline nanowire

Thermal conductivity of a single Bi$_{0.5}$Sb$_{1.5}$Te$_3$ single-crystalline nanowire

Liang Li[1]**, Chiming Jin**[2]**, Sichao Xu**[1]**, Jiyong Yang**[2]**, Haifeng Du**[2] **and Guanghai Li**[1,3]

[1] Key Laboratory of Materials Physics, Anhui Key Laboratory of Nanomaterials and Nanotechnology, Institute of Solid State Physics, Chinese Academy of Sciences, Hefei 230031, People's Republic of China
[2] High Magnetic Field Laboratory, Chinese Academy of Science, Hefei 230031, People's Republic of China
[3] University of Science and Technology of China, Hefei 230026, People's Republic of China

E-mail: ghli@issp.ac.cn and duhf@hmfl.ac.cn

Abstract

Single-crystalline Bi$_{0.5}$Sb$_{1.5}$Te$_3$ nanowires were fabricated by a template-assisted pulsed electrodeposition technique; the thermal conductivity of a single Bi$_{0.5}$Sb$_{1.5}$Te$_3$ nanowire of different diameters was characterized through a self-heating 3 ω method. The temperature-dependent resistance measurements prove the semiconductor behavior of the nanowires. The extremely low thermal conductivity of the nanowires was found compared with the corresponding bulk, and the Umklapp peaks shift to a higher temperature as the decreasing nanowire's diameter decreases, which qualitatively agrees with the theoretical calculations based on the Callaway model. The boundary scattering plays an important role in the reduction of the thermal conductivity and in the shift of the Umklapp peak of the Bi$_{0.5}$Sb$_{1.5}$Te$_3$ nanowires.

S Online supplementary data available from stacks.iop.org/NANO/25/415704/mmedia

Keywords: thermoelectric, thermal conductivity, Bi$_{2-x}$Sb$_x$Te$_3$, nanowires, boundary scattering

(Some figures may appear in colour only in the online journal)

1. Introduction

Thermoelectric materials, which can generate electrical power from thermal energy or convert electrical power into heating or cooling, are expected to play an increasingly important role in meeting future energy challenges [1, 2]. Generally, the efficiency of thermoelectric materials is qualified by figure of merit $ZT = S^2\sigma T/\kappa$, where S, σ, T and κ refer to the Seebeck coefficient, electrical conductivity, absolute temperature and thermal conductivity, respectively. To compete with traditional energy conversion technologies, thermoelectric materials should theoretically have a $ZT \geqslant 3$ [2]. Unfortunately, the interdependence and coupling between S, σ and κ of the traditional bulk thermoelectric materials makes it extremely difficult to fulfill this requirement [3].

Nanostructure engineering is considered to be one of the most effective ways to enhance the performance of currently promising thermoelectric materials. Previous experiments have demonstrated that the enhancement in ZT mainly comes from the reduction of thermal conductivity owing to the enhanced boundary scattering in nanostructures [4, 5]. This finding has inspired intensive investigation into the fabrication of nanostructured thermoelectric materials, such as Si nanowires, manganese silicide nanowires, Bi$_{2-x}$Sb$_x$Te$_3$ nanoplatelets and Bi$_2$Te$_3$ nanowires [6–9], in which Bi$_2$Te$_3$-based nanowires is the focus of interest due to their near-room-temperature applications and theory-predicated significant enhancement of ZT [10].

Bi$_2$Te$_3$-based nanowires, such as Bi$_2$Te$_3$, Bi$_{2-x}$Sb$_x$Te$_3$ and Bi$_2$Te$_{3-x}$Se$_x$, have been successfully fabricated by template-assisted electrodeposition techniques [11–15], while the electrodeposition of ternary Bi$_{2-x}$Sb$_x$Te$_3$ nanowires is relatively difficult because of the instability of antimony ions in water and the hardship in controlling a nanowire composition compared with binary compounds; the reported Bi$_{0.5}$Sb$_{1.5}$Te$_3$ nanowires are always polycrystalline [12, 16]. On the other

hand, the measurement of thermal conductivity of a single $Bi_{0.5}Sb_{1.5}Te_3$ nanowire is still lacking due to the difficulties in temperature measurement and heat flow control at the microscopic scale. Therefore, it is worth exploring the thermal conductivity of a single $Bi_{0.5}Sb_{1.5}Te_3$ nanowire with the anticipation of understanding its phonon transport mechanism and further designing the favorable nanostructure with a high thermoelectric efficiency.

In this paper, we report the fabrication of single-crystalline $Bi_{0.5}Sb_{1.5}Te_3$ nanowires by a pulsed electrodeposition technique and by the characterization of the thermal conductivity of single $Bi_{0.5}Sb_{1.5}Te_3$ nanowires using a self-heating 3 ω method [17–22]. An extremely low thermal conductivity was evidenced in the $Bi_{0.5}Sb_{1.5}Te_3$ nanowire compared with the corresponding bulk, and it was found that the Umklapp peaks shift to a higher temperature when the nanowire's diameter decreases, demonstrating an enhanced phonon-boundary scattering due to the reduction in the diameter of the $Bi_{0.5}Sb_{1.5}Te_3$ nanowires.

2. Experimental

2.1. Electrodeposition of Bi0.5Sb1.5Te3 nanowires

The anodic alumina membrane (AAM) was prepared using a two-step anodic anodization process, as previously described [23–26]. The electrodeposition was carried out in a three-electrode electrochemical cell in which a piece of graphite, a saturated calomel electrode and Au-sputtered AAMs served as a counter, a reference and a working electrode, respectively. An aqueous solution containing 1 M HNO_3, 0.002 M $Bi(NO_3)_3 \cdot 5H_2O$, 0.015 M TeO_2 and 0.02 M Sb_2O_3 was used as the electrolyte, and 0.3 M tartaric acid was used as the complexing agent. Before the electrodeposition, cyclic voltammogram (CV) experiments were performed to determine suitable voltage ranges for the deposition of the $Bi_{0.5}Sb_{1.5}Te_3$ nanowires. A millisecond-pulsed electrodeposition with pulses of 10 ms for reduction and 40 ms for relaxation was used to fabricate the nanowires, and an open-circuit potential was used in the relaxation time. The CV measurements and electrodeposition were carried out at room temperature using a CHI 660D electrochemical workstation.

2.2. Characterizations

The crystalline structure and morphology of the fabricated nanowires were characterized by x-ray diffraction (XRD, Philips PW 1700 with Cu K_α radiation), field-emission scanning electron microscopy (FE-SEM, FEI Sirion-200), transmission electron microscopy (TEM, H-800), selected area electron diffraction (SAED) and high-resolution transmission electron microscopy (HRTEM, JEOL-2010). The composition of the nanowires was determined by energy dispersive x-ray spectroscopy (EDX) attached to the TEM and by inductively coupled plasma atomic emission spectroscopy (ICP-AES, Thermo iCAP 6300). For the XRD measurements, the overfilled nanowires on the AAM surface were
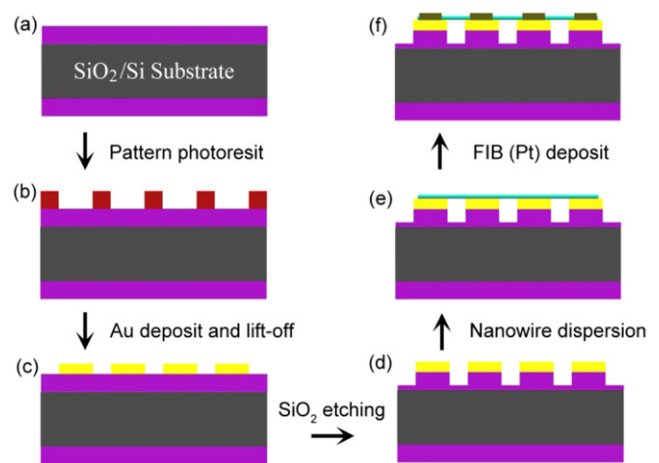

Figure 1. Schematic diagram of the fabrication process of the microdevice.

mechanically polished away. For the SEM observations, the AAM was dissolved with 2 M NaOH solution and then carefully rinsed with deionized water several times. For the TEM observations, the AAM was completely dissolved with a 2 M NaOH solution and then rinsed with absolute ethanol. For the ICP-AES analysis, the nanowires were dissolved in 0.5 mL concentrated HNO_3 and diluted to a final volume of 5 ml with deionized water.

2.3. Thermal conductivity measurement

A microdevice that consists of a single nanowire and of four-point-probe electrodes on the SiO_2/Si substrate was used to measure the thermal conductivity of the $Bi_{0.5}Sb_{1.5}Te_3$ nanowires. The schematic diagram of the fabricating process of the microdevice is shown in figure 1. Briefly, e-beam lithography was used to generate a photoresist pattern on a 500 nm thick SiO_2-coated Si substrate. After the e-beam evaporation of 5 nm thick Ti and 60 nm thick Au, a lift-off process follows to define the metal electrode pattern. To construct a suspended nanowire, which is necessary to avoid heat loss during the thermal conductivity measurement, about 200 nm SiO_2 steps were made by reactive ion etching. Then, a drop of the nanowire's suspension solution (the released nanowires were dispersed in ethanol using a low-power ultrasound) was dipped onto the microfabricated chip. Subsequently, the nanowire-dropped chip was transferred into an FEI FESEM/FIB dual beam system for defining a single nanowire that crossed the electrodes and for the deposition of top Pt-electrodes. It should be pointed out that Ga-doping or damage in the process of nanofabrication for the Pt-electrode deposition might form an amorphous. However, this amorphous is formed only on the upper surface of the nanowire at the electrodes, and the top Pt-electrodes are used only to fix the nanowire in the present study; it will not affect the measurements because the electrical conductivity of the Au electrodes that lie below the nanowire is much higher than the conductivity of the Pt electrodes that lie above the nanowire.
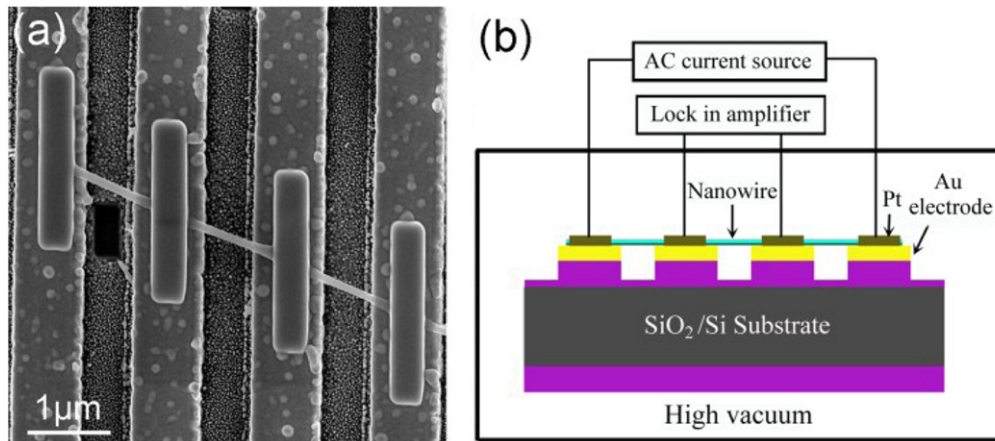
Figure 2. (a) SEM image of a suspended 67 nm $Bi_{0.5}Sb_{1.5}Te_3$ nanowire microdevice. (b) Schematic diagram of the 3ω measurement set-up.

A typical SEM image of the microdevice with a single $Bi_{0.5}Sb_{1.5}Te_3$ nanowire is shown in figure 2(a). The suspension of the nanowire on the Au steps and on the top Pt-electrodes can be clearly seen. The set-up for the thermal conductivity measurement is schematically illustrated in figure 2(b) in which a temperature fluctuation at a frequency of 2ω was generated when constant amplitude ac current $I_0\sin\omega t$ was applied through the suspended $Bi_{0.5}Sb_{1.5}Te_3$ nanowire, which resulted in a voltage fluctuation of 3ω across the nanowire. A lock-in amplifier was used to pick up the 3ω signal. If the condition $I_0^2 R'L/n^2\pi^2\kappa S \ll 1$ is fulfilled, the third harmonic voltage across the nanowire with an accuracy of 1.2% can be described by the equation [17, 18, 22]:

$$V_{3\omega,\,rms} \cong \frac{\sqrt{2}\,I_0^3 RR'L}{\pi^4\kappa S} \qquad (1)$$

where R, R', L, κ and S are the resistance, temperature gradient of the resistance, length, thermal conductivity and cross-sectional area of the suspended nanowire, respectively. To fulfill the above-mentioned condition, the input current must be within tens of the μA, according to the previous works [19, 21, 22, 27, 28].

3. Results and discussion

3.1. Characterizations of nanowires

To determine the growth condition of the $Bi_{2-x}Sb_xTe_3$ nanowires, the CV scanning of the electrolytes with and without the Sb were firstly performed, and the results are shown in figure 3. Three reduction waves situated at about 0.3, −0.05 and −0.7 V (the labels A, B and C in the Bi-Te bath of figure 3), correspond, respectively, to the reduction of $HTeO_2^+$ and Bi^{3+} to Bi_2Te_3; the formation of Bi_2Te_3 via an intermediate step and the onset of hydrogen evolution [29] can be clearly seen for the electrolyte without Sb. However, for the electrolyte with Sb, three major reduction waves (the labels D, E and F in the Bi-Sb-Te bath of figure 3) at about −0.1, −0.36 and −0.7 V can be observed in which peak D is
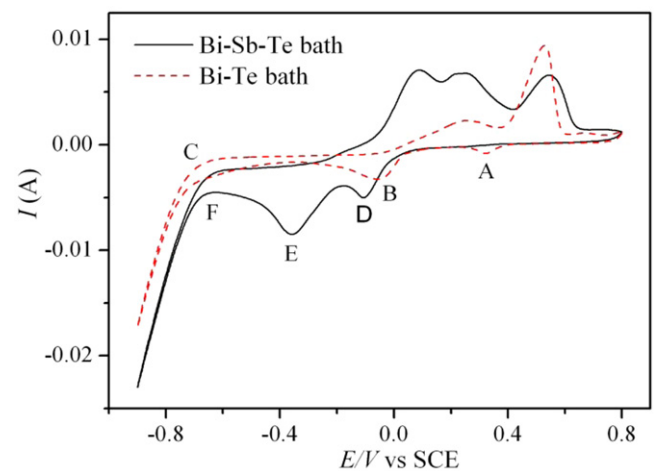

Figure 3. CV curves of the electrolyte for the deposition of the Bi-Sb-Te ternary alloy and Bi-Te binary alloy. The scan rate is $0.04\ V\ s^{-1}$.

considered and mainly comes from the formation of the Bi_2Te_3 alloy. Peak E corresponds to the co-deposition of Bi, Sb and Te, and peak F is the onset of the hydrogen evolution. It is worth noting that the peak value for the formation of Bi_2Te_3 in the Bi-Sb-Te bath is more negative than that in the Bi-Te bath and is attributed to the slight deposition of Sb. From these results, we can conclude that the deposition of $Bi_{2-x}Sb_xTe_3$ is more favorable at the greater potential negativity than −0.1 V, and it was found that the stoichiometric $Bi_{0.5}Sb_{1.5}Te_3$ nanowires can be fabricated at the potential of −0.35 V. The corresponding ICP-AES analysis shows that the resulting Bi-Sb-Te nanowires have the composition of 10.3 Bi, 30.1 Sb and 59.6 Te at %, which is close to the stoichiometric formula of $Bi_{0.5}Sb_{1.5}Te_3$.

Figure 4 shows the typical SEM images of $Bi_{0.5}Sb_{1.5}Te_3$ nanowires with three different diameters after the removal of AAM through etching in a 2 M NaOH solution for several minutes. The diameters of the nanowires were determined to be 67, 124 and 282 nm, respectively. Figure 5 shows the XRD patterns of the $Bi_{0.5}Sb_{1.5}Te_3$ nanowire arrays with the AAMs in which only one sharp diffraction peak can be observed in

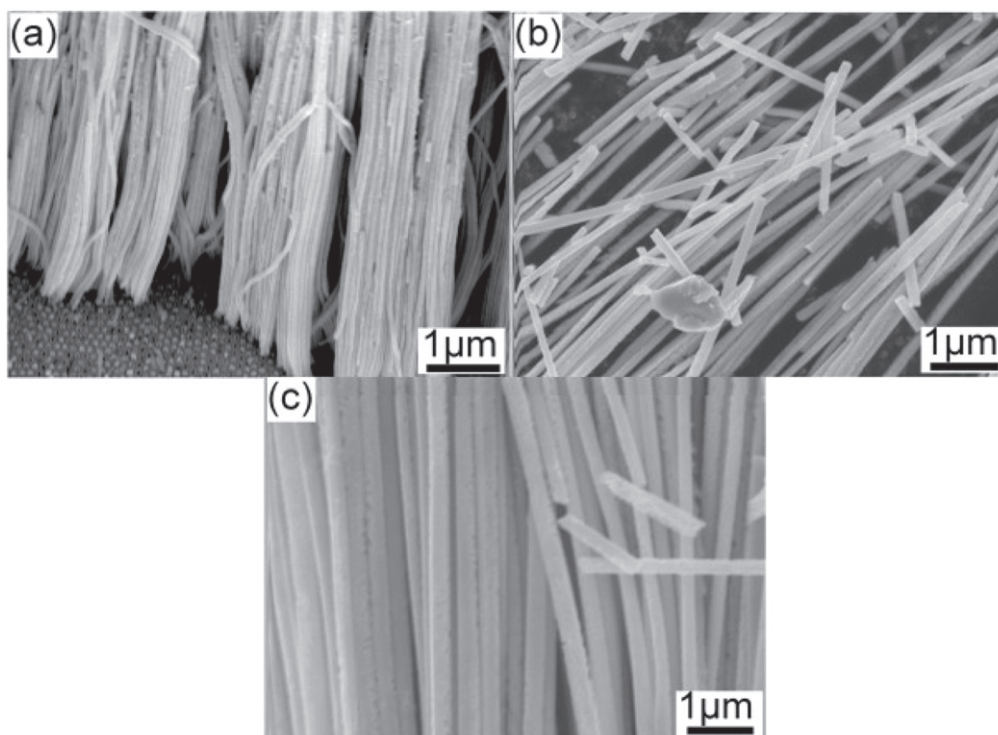**Figure 4.** SEM images of $Bi_{0.5}Sb_{1.5}Te_3$ nanowires with diameters of (a) 67, (b) 124 and (c) 282 nm after removing the AAM.

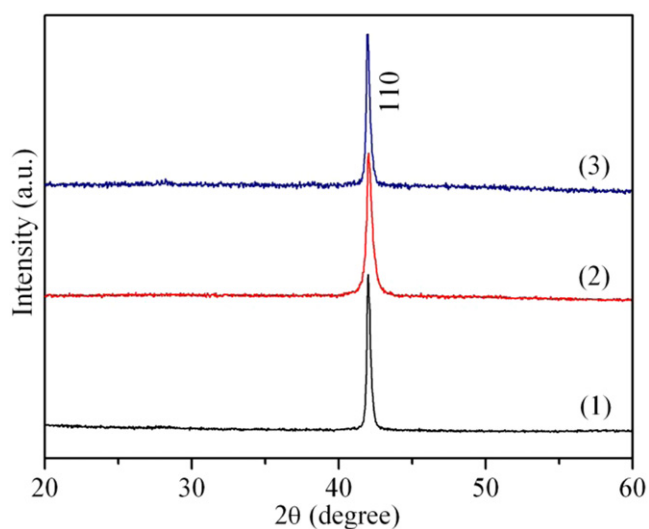**Figure 5.** XRD patterns of the $Bi_{0.5}Sb_{1.5}Te_3$ nanowire arrays with diameters of (1) 67, (2) 124 and (3) 282 nm.

each XRD pattern; this indicates that the nanowires with different diameters all have a highly preferential orientation along the [110] direction. Other diffraction peaks related to elemental Bi, Sb, Te and their binary compounds were not observed, which indicates the formation of a complete single phase $Bi_{0.5}Sb_{1.5}Te_3$.

Figure 6(a) shows a typical TEM image of a single $Bi_{0.5}Sb_{1.5}Te_3$ nanowire after complete removal from the AAM. One can see that the nanowire has a diameter of 67 nm. The corresponding SAED pattern proves the single crystalline of the nanowire, and the growth direction is [110], as shown

in figure 6(a). The HRTEM image of the nanowire further confirms the single crystalline of the $Bi_{0.5}Sb_{1.5}Te_3$ nanowire in which the interplanar spacing of 0.202 nm matches well with the (0015) plane of the $Bi_{0.5}Sb_{1.5}Te_3$ phase, which indicates that the nanowire grows along the [110] direction (figure 6(b)); this is in agreement with the XRD result. The corresponding EDS analysis shows the existence of only Bi, Sb and Te (along with the presence of Cu and C from the holey-carbon-coated copper grid in figure 6(c)); the quantitative EDS analysis shows that the ratio of Bi:Sb:Te is about 9.5:28.2:62.3, which is close to the ICP-AES result.

3.2. Electrical transport properties

For electrical and 3 ω signal measurements, the microdevice was placed in a cryogenic and vacuum system (Edward), which also acts as a shielding box. In order to measure the resistance of the $Bi_{0.5}Sb_{1.5}Te_3$ nanowires, the four-point-probe method was used for the *I-V* measurements, and the resistance can be obtained from the slope of the *I-V* curves. Figure 7(a) shows the typical *I-V* curves of the 67 nm $Bi_{0.5}Sb_{1.5}Te_3$ nanowire, and a perfectly linear relationship between the current and the voltage can be seen. The same results were also found for 124 and 282 nm $Bi_{0.5}Sb_{1.5}Te_3$ nanowires (see figures S1(a, b) and S2(a, b) of the supporting information). Figure 7(b) shows the temperature-dependent electrical resistance of the $Bi_{0.5}Sb_{1.5}Te_3$ nanowire with different diameters. One can see that the resistances decrease nonlinearly with the increasing temperature, displaying a typical semiconductor behavior. Also, the temperature gradient of the resistances ($R' = dR/dT$) is not a constant over the entire temperature range. Therefore, to avoid errors in the
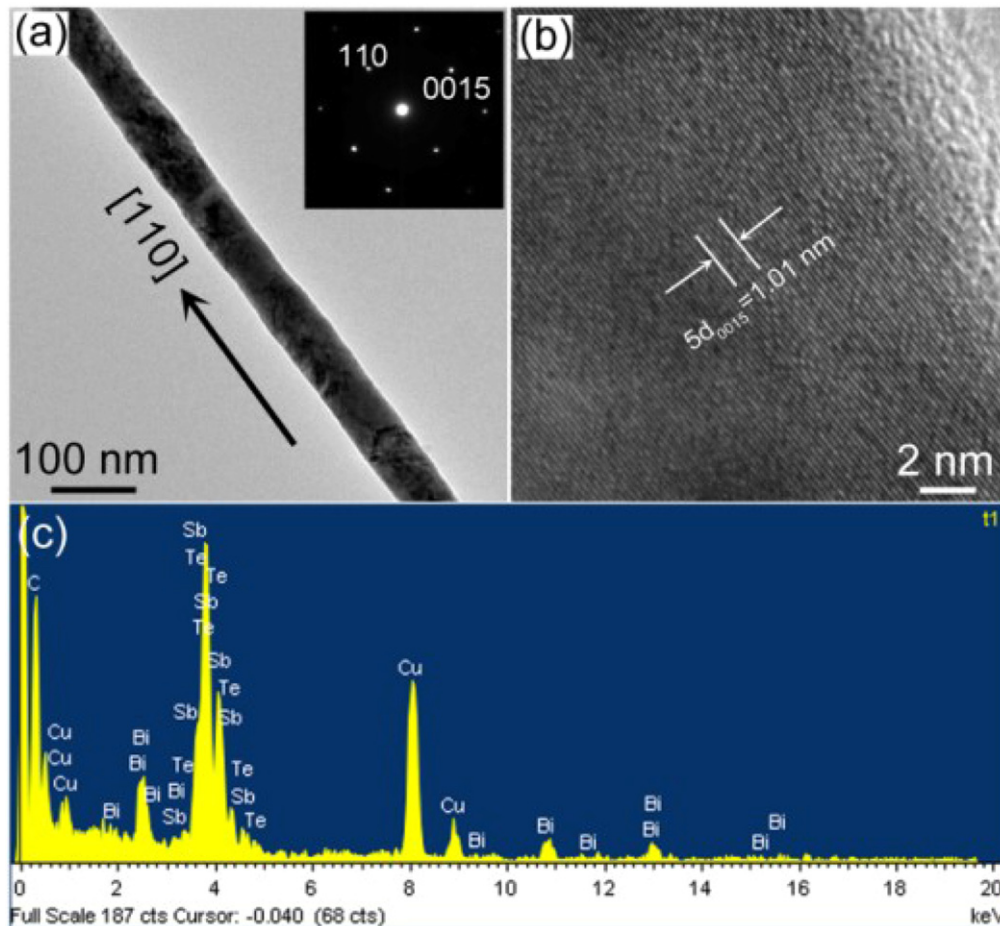
Figure 6. (a) TEM and (b) HRTEM images of a single $Bi_{0.5}Sb_{1.5}Te_3$ nanowire (67 nm) and the (c) EDS spectrum. The inset in (a) is the corresponding SAED pattern.

calculation of the thermal conductivity, the R' values were calculated from the slope with a combined linear and estimator function [20] (see figures S3–S5).

Although the four-probe method for the *I-V* measurements cannot judge the ohmic contact, the electrode's contacts were either ohmic or unable to affect the 3ω measurement with the four-probe method. According to equation (1), the $V_{3\omega}$ is proportional to the cube of input ac current I_0. The $V_{3\omega}$ signal was measured at different temperatures to check this relationship. For example, the $V_{3\omega}$ of the 67 nm $Bi_{0.5}Sb_{1.5}Te_3$ nanowire as a function of the input ac current at 50 and 300 K is shown in figure 8, which demonstrates that there is a linear relationship between $V_{3\omega}$, the ac current amplitude (I_0^x) and the resultant exponent, x, from the fitting data, which is about 2.87 and 2.96 at 50 K and 300 K respectively; this is very close to the ideal value of 3. Similar results are also found in the 124 and 282 nm $Bi_{0.5}Sb_{1.5}Te_3$ nanowires (see figures S1(c, d) and S2(c, d)). This result indicates that the heat produced by the input ac current has mostly diffused through the suspended nanowire, and the heat loss is very limited, which demonstrates that the calculated thermal conductivity using the data measured by the 3 ω method is reliable [19].

3.3. Thermal conductivity

The calculated thermal conductivity using equation (1) at a temperature range of $20 \sim 320$ K of a single $Bi_{0.5}Sb_{1.5}Te_3$ nanowire with different diameters is shown in figure 9(a). One can see that the thermal conductivities of the $Bi_{0.5}Sb_{1.5}Te_3$ nanowires decrease with the decreasing nanowire diameter at all of the measured temperatures and are about several times lower than that of the bulk material at room temperature [5] (see discussion below). The enhanced boundary scattering in the nanowires is considered to be the main reason for the reduced thermal conductivity [30]. From figure 9(a), one also can see that the thermal conductivity of the $Bi_{0.5}Sb_{1.5}Te_3$ nanowire firstly increases with the increasing temperature at a low temperature; after reaching a peak value, it finally decreases at a high temperature. This peak is the so-called Umklapp peak and is at about 150, 70 and 50 K for 67, 124 and 282 nm nanowires, respectively, which are all higher than that of the bulk nanostructured $Bi_{0.5}Sb_{1.5}Te_3$ pellets (about 20 K) [31]. The fact that the Umklapp peak of the $Bi_{0.5}Sb_{1.5}Te_3$ nanowires shifts to a high temperature with the decreasing diameter suggests that the phonon-phonon Umklapp scattering, which decreases the thermal conductivity, is suppressed because of the enhanced phonon boundary scattering via the size effect.
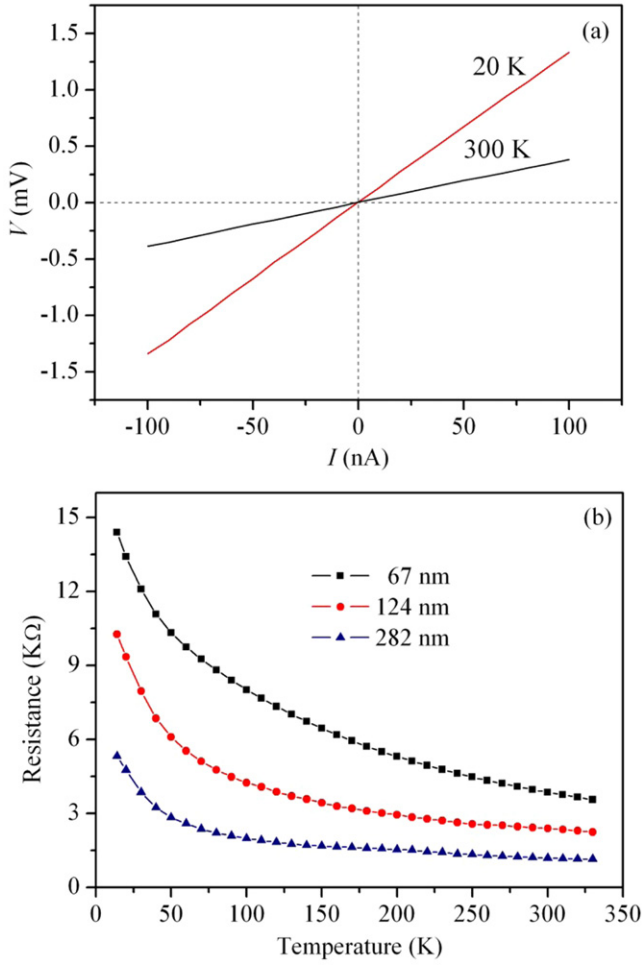
Figure 7. (a) *I–V* curves of a 67 nm Bi$_{0.5}$Sb$_{1.5}$Te$_3$ nanowire at different temperatures. (b) Temperature-dependent resistance of a single Bi$_{0.5}$Sb$_{1.5}$Te$_3$ nanowire with different diameters.
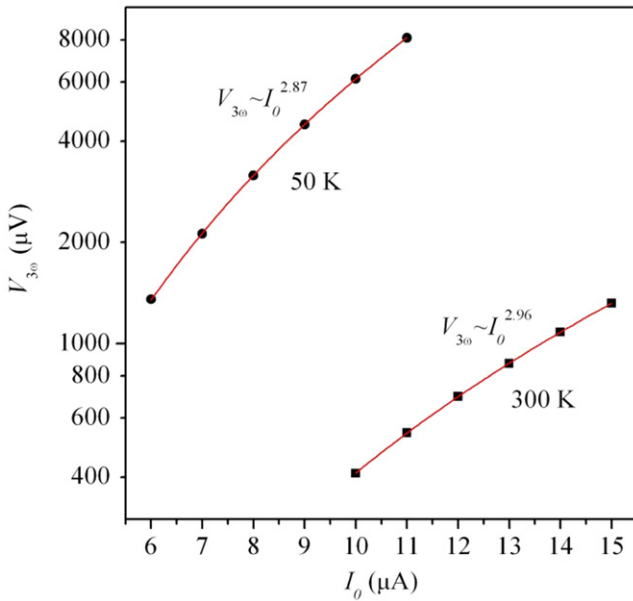

Figure 8. 3 *ω* signal as a function of current at 50 and 300 K.

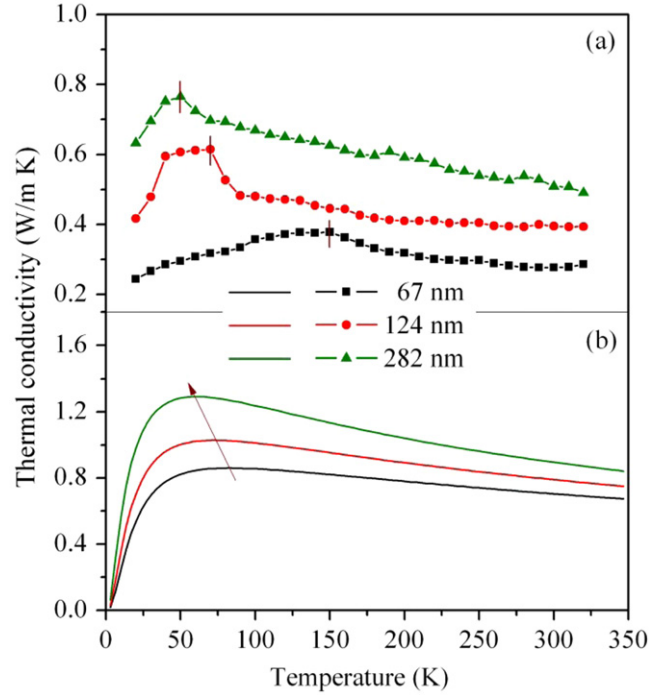**Figure 9.** Temperature-dependent thermal conductivity of Bi$_{0.5}$Sb$_{1.5}$Te$_3$ single nanowires with different diameters calculated from (a) equation (1) and the (b) Callaway model.

In order to better understand the origins of the reduction in thermal conductivities and the shift of the Umklapp peak, we consider the frequency-dependent relaxation time of phonons according to the Mathiessen's rule:

$$\tau^{-1}(\omega) = A\omega^4 + B\omega^2 T e^{(-\theta_D/3T)} + \tau_b^{-1} \qquad (2)$$

where $A\omega^4$, $B\omega^2 T\exp(-\theta_D/3T)$ and τ_b^{-1} are the point-defect scattering, phonon-phonon Umklapp scattering and boundary scattering, respectively; A and B are independent of temperature $\tau_b^{-1} = \upsilon/d$ where d is the critical size of the sample. In the present study, the fitting parameters of υ, A, B and θ_D taken from [32] were used to calculate the thermal conductivities of nanowires by the simple Callaway model [33, 34]. The calculation results are shown in figure 9(b). One can see that the thermal conductivities are indeed smaller than the corresponding bulk material (0.70, 0.79 and 0.89 W mK^{-1} at 300 K for 67, 124 and 282 nm nanowires, respectively, and 1.4 W mK^{-1} for the bulk) [5]. From figure 9(b), one also can see that the Umklapp peak temperature of the nanowires shifts to a high temperature with the decreasing nanowire diameter and is at about 83, 72 and 58.5 K, respectively. Also, it is higher than the corresponding bulk (at 20 K). Because the parameters A and B are obtained from the bulk material, one can thus conclude that the boundary scattering truly plays an important role in the reduction of the thermal conductivity and the suppression of the Umklapp peaks of the nanowires. It is worth noting that the thermal conductivity calculated from the Callaway model is higher than that from equation (1). Some possible reasons that might account for the discrepancy are: (1) the roughness on the nanowire's

surface may act as secondary scattering phases [4], as proved by a recent theoretical and experimental study on Si nanowires in which the surface roughness has great influence on the thermal conductivity [35, 36]; (2) the parameters obtained from the bulk did not take into account the crystal anisotropy (the $Bi_{0.5}Sb_{1.5}Te_3$ with a rhombohedral structure is highly anisotropic); (3) the existence of other defect-scattering processes that extend beyond mass fluctuation and strain field scattering [37] and (4) the ignored carrier-phonon scattering in the calculation. Further work should be focused on the above-mentioned reasons.

4. Conclusions

In summary, single-crystalline and highly preferentially oriented $Bi_{0.5}Sb_{1.5}Te_3$ nanowires with different diameters have been prepared by a pulsed electrodeposition based on the AAM. Unusually low thermal conductivity on a single $Bi_{0.5}Sb_{1.5}Te_3$ nanowire was determined using the self-heating 3ω method. It was found that the electrical resistance of the $Bi_{0.5}Sb_{1.5}Te_3$ nanowires decreases with the increasing temperature, and the thermal conductivity firstly increases and then decreases with the increasing temperature. In addition, the Umklapp peak shifts to a high temperature with the decreasing diameter, which is qualitatively in agreement with our theoretical calculation based on a simple Callaway model. The enhanced surface phonon scattering is considered to be responsible for the reduction in the thermal conductivity. Our results will shed some light on the fabrication and understanding of the thermal transport mechanism of other 1D thermoelectric materials such as superlattice nanowires. Further work concerning the *ZT* of $Bi_{0.5}Sb_{1.5}Te_3$ nanowires and the optimization of the thermoelectric performance based on the data obtained by the 3ω technique is underway.

Acknowledgments

References

[1] Dresselhaus M S, Chen G, Tang M Y, Yang R G, Lee H, Wang D Z, Ren Z F, Fleurial J P and Gogna P 2007 *Adv. Mater.* **19** 1043–53
[2] Hochbaum A I and Yang P D 2010 *Chem. Rev.* **110** 527–46
[3] Vineis C J, Shakouri A, Majumdar A and Kanatzidis M G 2010 *Adv. Mater.* **22** 3970–80
[4] Hochbaum A I, Chen R K, Delgado R D, Liang W J, Garnett E C, Najarian M, Majumdar A and Yang P D 2008 *Nature* **451** 163–7
[5] Poudel B, Hao Q, Ma Y, Lan Y, Minnich A, Yu B, Yan X, Wang D, Muto A and Vashaee D 2008 *Science* **320** 634–8
[6] Azeredo B, Sadhu J, Ma J, Jacobs K, Kim J, Lee K, Eraker J, Li X, Sinha S and Fang N 2013 *Nanotechnology* **24** 225305
[7] Pokhrel A, Degregorio Z P, Higgins J M, Girard S N and Jin S 2013 *Chem. Mater.* **25** 632–8
[8] Scheele M, Oeschler N, Veremchuk I, Reinsberg K-G, Kreuziger A-M, Kornowski A, Broekaert J, Klinke C and Weller H 2010 *ACS Nano* **4** 4283–91
[9] Hsin C-L, Wingert M, Huang C-W, Guo H, Shih T-J, Suh J, Wang K, Wu J, Wu W-W and Chen R 2013 *Nanoscale* **5** 4669–72
[10] Hicks L D and Dresselhaus M S 1993 *Phys. Rev.* B **47** 12727–31
[11] Martin-Gonzalez M, Snyder G J, Prieto A L, Gronsky R, Sands T and Stacy A M 2003 *Nano Lett.* **3** 973–7
[12] Martin-Gonzalez M, Prieto A L, Gronsky R, Sands T and Stacy A M 2003 *Adv. Mater.* **15** 1003–6
[13] Li L, Yang Y W, Huang X H, Li G H and Zhang L D 2006 *Nanotechnology* **17** 1706–12
[14] Sander M S, Prieto A L, Gronsky R, Sands T and Stacy A M 2002 *Adv. Mater.* **14** 665–7
[15] Tian M L, Ning W, Qu Z, Du H F, Wang J and Zhang Y H 2013 *Sci. Rep.* **3** 1212
[16] Li X H, Koukharenko E, Nandhakumar I S, Tudor J, Beeby S P and White N M 2009 *Phys. Chem. Chem. Phys.* **11** 3584–90
[17] Lu L, Yi W and Zhang D 2001 *Rev. Sci. Instrum.* **72** 2996–3003
[18] Choi T Y, Poulikakos D, Tharian J and Sennhauser U 2005 *Appl. Phys. Lett.* **87** 013108
[19] Lee S-Y, Kim G-S, Lee M-R, Lim H, Kim W-D and Lee S-K 2013 *Nanotechnology* **24** 185401
[20] Lee S-Y, Lee M-R, Park N-W, Kim G-S, Choi H-J, Choi T-Y and Lee S-K 2013 *Nanotechnology* **24** 495202
[21] Li G, Liang D, Qiu R L and Gao X 2013 *Appl. Phys. Lett.* **102** 043104
[22] Choi T-Y, Poulikakos D, Tharian J and Sennhauser U 2006 *Nano Lett.* **6** 1589–93
[23] Jessensky O, Muller F and Gosele U 1998 *Appl. Phys. Lett.* **72** 1173–5
[24] Zhang Y, Li G H, Wu Y C, Zhang B, Song W H and Zhang L 2002 *Adv. Mater.* **14** 1227–30
[25] Li L, Yang Y W, Li G H and Zhang L D 2006 *Small* **2** 548–53
[26] Dou X, Zhu Y, Huang X, Li L and Li G 2006 *J. Phys. Chem.* B **110** 21572–5
[27] Holtzman A, Shapira E and Selzer Y 2012 *Nanotechnology* **23** 495711
[28] Finefrock S W, Wang Y, Ferguson J B, Ward J V, Fang H, Pfluger J E, Dudis D S, Ruan X and Wu Y 2013 *Nano Lett.* **13** 5006–12
[29] Lee J, Farhangfar S, Cagnon L, Scholz R, Gösele U and Nielsch K 2008 *Nanotechnology* **19** 365701
[30] Li D, Wu Y, Kim P, Shi L, Yang P and Majumdar A 2003 *Appl. Phys. Lett.* **83** 2934–6
[31] Dyck J S, Mao B D, Wang J W, Dorroh S and Burda C 2012 *J. Electron. Mater.* **41** 1408–13
[32] Katcho N A, Mingo N and Broido D 2012 *Phys. Rev.* B **85** 115208
[33] Callaway J 1959 *Phys. Rev.* **113** 1046–51
[34] Mingo N, Yang L, Li D and Majumdar A 2003 *Nano Lett.* **3** 1713–6
[35] Sadhu J and Sinha S 2011 *Phys. Rev.* B **84** 115450
[36] Ghossoub M, Valavala K, Seong M, Azeredo B, Hsu K, Sadhu J, Singh P and Sinha S 2013 *Nano Lett.* **13** 1564–71
[37] Balandin A 2000 *Phys. Low-Dimens. Struct.* **1/2** 1–28